Thermodynamics of hexagonal-close-packed iron under Earth's core conditions

D. Alfè[1], G. D. Price[1] and M. J. Gillan[2]

[1]Research School of Geological and Geophysical Sciences
Birkbeck and University College London
Gower Street, London WC1E 6BT, UK

[2]Physics and Astronomy Department, University College London
Gower Street, London WC1E 6BT, UK

The free energy and other thermodynamic properties of hexagonal-close-packed iron are calculated by direct *ab initio* methods over a wide range of pressures and temperatures relevant to the Earth's core. The *ab initio* calculations are based on density-functional theory in the generalised-gradient approximation, and are performed using the projector augmented wave (PAW) approach. Thermal excitation of electrons is fully included. The Helmholtz free energy consists of three parts, associated with the rigid perfect lattice, harmonic lattice vibrations, and anharmonic contributions, and the technical problems of calculating these parts to high precision are investigated. The harmonic part is obtained by computing the phonon frequencies over the entire Brillouin zone, and by summation of the free-energy contributions associated with the phonon modes. The anharmonic part is computed by the technique of thermodynamic integration using carefully designed reference systems. Detailed results are presented for the pressure, specific heat, bulk modulus, expansion coefficient and Grüneisen parameter, and comparisons are made with values obtained from diamond-anvil-cell and shock experiments.

PACS numbers: 71.15.-m 64.10.+h 62.50.+p

I. INTRODUCTION

Ab-initio techniques based on density-functional theory (DFT) have played a key role for several years in the study of matter under extreme conditions [1]. With recent progress in the direct *ab initio* calculation of thermodynamic free energies [2–4], there is now great scope for the systematic and accurate calculation of thermodynamic properties over a wide range of conditions. We present here extensive DFT calculations of the free energy of hexagonal-close-packed (h.c.p.) iron under Earth's core conditions, which we have used to obtain results for a number of other thermodynamic quantities, including the bulk modulus, expansion coefficient, specific heat and Grüneisen parameter. For some of these we can make direct comparisons with experimental data, which support the accuracy and realism of the calculations; for others, the calculations supply information that is not yet available from experiments. An important ambition of the work is to determine thermodynamic functions without making any significant statistical-mechanical or electronic-structure approximations, other than those required by DFT itself, and we shall argue that we come close to achieving this. The techniques we have developed are rather general, and we believe they will find application to many other problems concerning matter under extreme conditions.

The importance of understanding the high-pressure and high-temperature properties of iron can be appreciated by recalling that the Earth's core accounts for about 30 % of the mass of the entire Earth, and consists mainly of iron [5]. In fact, the liquid outer core is somewhat less dense than pure iron, and is generally accepted to contain light impurities such as S, O, Si or H [6]; probably the density of the solid inner core is also significantly reduced by impurities [7,8]. Nevertheless, the thermodynamic properties of pure iron are fundamental to understanding the more complex real material in the core, and a large experimental effort has been devoted to measuring them. The difficulties are severe, because the pressure range of interest extends from 100 GPa up to nearly 400 GPa, and the temperature goes from *ca.* 3000 K to perhaps 7000 K – the temperature at the centre of the core is subject to an uncertainty of at least 1000 K.

Static compression experiments with the diamond anvil cell (DAC) have been performed on Fe up to 300 GPa at room temperature [9], and DAC experiments at temperatures as high as 3700 K have been reported up to 200 GPa [10–18]. Our present knowledge of the phase diagram of Fe comes mainly from these experiments, though there are still controversies. For pressures p above *ca.* 60 GPa and temperatures T below *ca.* 1500 K it is generally accepted that the stable phase is hexagonal close packed (h.c.p.). Recent DAC diffraction experiments [18] indicate that h.c.p. is actually stable for all temperatures up to the melting line for $p > 60$ GPa, but earlier work claimed that there is another phase, usually called β, in a region below the melting line for pressures above *ca.* 40 GPa. The existing evidence suggests that, if the β-phase is thermodynamically stable, its structure could either be double-h.c.p. [14,15] or orthorhombic [17], and in either case is closely related to the usual h.c.p. structure. According to very recent theoretical work [19], h.c.p. is thermodynamically slightly more stable than double-h.c.p. at Earth's core pressures and temperatures. The evidence for the stability of h.c.p. over much of the high-temperature/high-pressure phase diagram is our motivation for concentrating on this phase in the present work.

DAC measurements have given some information about thermodynamic quantities up to pressures of a few tens of GPa, but beyond this shock experiments (see e.g. Refs. [20–22]) have no competitors. These experiments give direct values of the pressure as a function of volume [21] on the Hugoniot curve, and have also been used to obtain information about the adiabatic bulk modulus and some other thermodynamic quantities on this curve. These data will be important in validating our calculations. Temperature is difficult to measure reliably in shock experiments [22], and we believe that our *ab initio* results may be valuable in providing the needed calibration.

The difficulties and uncertainties of experiments have stimulated many theoretical efforts. Some of the theoretical work has been based on simple atomistic models, such as a representation of the total energy as a sum of pair potentials [23], or the more sophisticated embedded-atom model [24]. Such models can be useful, but for accuracy and reliability they cannot match high-quality *ab initio* calculations based on DFT [25]. The accuracy of DFT depends very much on the approximation used for the electronic exchange-correlation energy E_{xc}. It is known that the local density approximation (LDA) is not fully satisfactory for Fe [26], but that modern generalised-gradient approximations (GGA) reproduce a wide range of properties very accurately. These include the equilibrium lattice parameter, bulk modulus and magnetic moment of body-centred cubic (b.c.c.) Fe at ambient pressures [27–29], and the phonon dispersion relations of the b.c.c. phase [19]. There has been much DFT work on different crystal structures of Fe at high pressures, and experimental low-temperature results for the pressure as a function of volume $p(V)$ up to $p = 300$ GPa for the h.c.p. structure are accurately predicted [9]. Further evidence for the accuracy of DFT comes from the successful prediction of the b.c.c. to h.c.p. transition pressure [27,28], and comparison with the measured phonon density of states of the h.c.p. phase up to pressures of ~ 150 GPa [30]. With *ab-initio* molecular dynamics, DFT calculations can also be performed on the liquid state, and we have reported extensive calculations both on pure liquid Fe [29,31,32] and on liquid Fe/S and Fe/O alloys [33–35].

Recently, work has been reported [8,36] in which the thermal properties of close-packed crystalline Fe under Earth's core conditions are calculated using *ab initio* methods. In fact, the work itself was based on a tight-binding representation of the total energy, but this was parameterised using extensive *ab initio* data. The authors did not attempt to perform the statistical-mechanical calculations exactly, but instead used the so-called 'particle in a cell' approximation [37], in which vibrational correlations between atoms are ignored. In spite of these limitations, the work yielded impressive agreement with shock data. We shall make comparisons with this work at various points in the present paper.

The present DFT work is based on the GGA known as Perdew-Wang 1991 [38,39]. The choice of functional for exchange-correlation energy E_{xc} exactly determines the free energy and all other thermodynamic quantities. By this, we simply mean that E_{xc} exactly determines the total energy of the system $U(\mathbf{R}_1, \ldots \mathbf{R}_N)$ as a function of atomic positions $\{\mathbf{R}_i\}$, and the standard formulas of statistical mechanics express the free energy F exactly in terms of $U(\mathbf{R}_1, \ldots \mathbf{R}_N)$. The calculation of U from E_{xc} has been discussed over many years by many authors. The present work is based on the projector-augmented-wave (PAW) implementation of DFT [32,40,41], which is an all-electron technique similar to other standard implementations such as full-potential linear augmented plane waves (FLAPW) [42], as well as being closely related to the ultrasoft pseudopotential (USPP) method [45]. In principle, PAW allows one to compute U with any required precision from a given E_{xc}. In practical tests on Fe and other systems [32,41], the technique has been shown to yield results that are almost indistinguishable from calculations based on FLAPW, USPP and other DFT implementations. We aim to demonstrate in this work that F can also be computed from the *ab initio* $U(\mathbf{R}_1, \ldots \mathbf{R}_N)$ to any required precision.

To clarify the precision we are aiming for in the calculation of F, we need to explain that one of the wider objectives of this work is the ab initio determination of the high-pressure melting properties of Fe, a brief report on which has been published elsewhere [43] (see also Ref. [44]). Our approach to melting starts from the basic principle that at coexistence the Gibbs free energies $G_{\mathrm{sol}}(p, T)$ and $G_{\mathrm{liq}}(p, T)$ of solid and liquid are equal. But for a given pressure, the curves of $G_{\mathrm{sol}}(p, T)$ and $G_{\mathrm{liq}}(p, T)$ cross at a shallow angle. The difference of slopes $(\partial G_{\mathrm{sol}}/\partial T)_p = S_{\mathrm{sol}}$ and $(\partial G_{\mathrm{liq}}/\partial T)_p = S_{\mathrm{liq}}$ is equal to the entropy of fusion $S_{\mathrm{m}} \equiv S_{\mathrm{liq}} - S_{\mathrm{sol}}$, which is comparable to k_{B} per atom. This means that to get the melting temperature within an error of δT, the non-cancelling errors in G_{sol} and G_{liq} must not exceed *ca.* $k_{\mathrm{B}} \delta T$. Ideally, we should like to calculate the melting temperature to within *ca.* 100 K, so that non-cancelling errors must be reduced to the level of *ca.* 10 meV. Our original ambition for the present work on h.c.p. Fe was to obtain F from the given *ab-initio* $U(\mathbf{R}_1, \ldots \mathbf{R}_N)$ to this precision, and to demonstrate that this has been achieved. As we shall see, this target has probably not been attained, but we miss it by only small factor, which will be estimated.

We shall present results for thermodynamic quantities for pressures $50 < p < 400$ GPa and temperatures $2000 < T < 6000$ K. This is a far wider range than is strictly needed for understanding the inner core, where pressures span the range $330 < p < 364$ GPa and T is believed to be in the region of $5000 - 6000$ K. However, the wider range is essential in making comparisons with the available laboratory data. We set the lower limit of 2000 K for our T range because this is the lowest T that has been proposed for equilibrium between the h.c.p. crystal and the liquid (at lower T, melting occurs from the f.c.c. phase).

In the next Section, we summarize the *ab initio* techniques, and give a detailed explanation of the statistical-mechanical techniques. The three Sections after that present our investigations of the three main components of the free energy, associated with the rigid perfect lattice, harmonic lattice vibrations, and anharmonic contributions, probing in each case the technical measures that must be taken to achieve our target precision. Sec. 6 reports our results for all the thermodynamic quantities derived from the free energy, with comparisons wherever possible with experimental measurements and previous theoretical values. Overall discussion and conclusions are given in Sec. 7. The implications of our results for deepening our understanding of the Earth's core will be analysed elsewhere.

II. TECHNIQUES

A. Ab initio techniques

The use of DFT to calculate the energetics of many-atom systems has been extensively reviewed [25]. Thermal electronic excitations play a crucial role in the current work, and we handle these using the standard methods of finite-temperature DFT developed by Mermin [46–48]. The fundamental quantity is the electronic free energy $U(\mathbf{R}_1, \ldots \mathbf{R}_N; T_{\rm el})$ calculated at electronic temperature $T_{\rm el}$ with the N nuclei fixed at positions $\mathbf{R}_1, \ldots \mathbf{R}_N$. This is given by $U = E - TS$, where the DFT energy E is the usual sum of kinetic, electron-nucleus, Hartree, and exchange-correlation terms, and S is the electronic entropy, given by the independent-electron formula $S = -2k_{\rm B}T_{\rm el} \sum_i [f_i \ln f_i + (1 - f_i)\ln(1 - f_i)]$, with f_i the thermal (Fermi-Dirac) occupation number of orbital i. The electronic kinetic energy and other parts of E also contain the occupation numbers. In exact DFT, the exchange-correlation (free) energy $E_{\rm xc}$ has an explicit dependence on $T_{\rm el}$. Very little is known about this dependence, and we assume here that $E_{\rm xc}$ has its zero-temperature form.

Throughout this work, we treat the statistical mechanics of the nuclei in the classical limit, and we show later that quantum corrections are negligible under the conditions of interest. The Helmholtz free energy of the whole system is then:

$$F = -k_{\rm B}T \ln \left\{ \frac{1}{N!\Lambda^{3N}} \int d\mathbf{R}_1 \ldots d\mathbf{R}_N \, \exp\left[-\beta U(\mathbf{R}_1, \ldots \mathbf{R}_N; T_{\rm el})\right] \right\} , \tag{1}$$

where $\Lambda = h/(2\pi M k_{\rm B}T)^{1/2}$ is the thermal wavelength, with M the nuclear mass, and $\beta = 1/k_{\rm B}T$. In practice, the electronic and nuclear degrees of freedom are in thermal equilibrium with each other, so that $T_{\rm el} = T$, but it will be useful to keep the logical distinction between the two. Although $U(\mathbf{R}_1, \ldots \mathbf{R}_N)$ is really a *free* energy, we will generally call it the total energy function, to avoid confusion with the overall free energy F.

The PAW implementation of DFT has been described in detail in previous papers [40,41]. The present calculations were done using the VASP code [49,50]. The details of the core radii, augmentation-charge cut-offs, etc are exactly as in our recent PAW work on liquid Fe [32]. Our division into valence and core states is also the same: the $3p$ electrons are treated as core states, but their response to the high compression is represented by an effective pair potential, with the latter constructed using PAW calculations in which the $3p$ states are explicitly included as valence states. Further technical details are as follows. All the calculations are based on the form of GGA known as Perdew-Wang 1991 [38,39]. Brillouin-zone sampling was performed using Monkhorst-Pack special points [51], and the detailed form of sampling will be noted where appropriate. The plane-wave cut-off of 300 eV was used, exactly as in our PAW work on liquid Fe.

B. Components of the free energy

Our *ab initio* calculations of thermodynamic properties are based on a separation of the Helmholtz free energy F into the three components mentioned in the Introduction, which are associated with the rigid perfect crystal, harmonic lattice vibrations, and anharmonic contributions.

To explain this separation, we start from the expression for F given in Eqn (1). We let $F_{\rm perf}(T_{\rm el}) \equiv U(\mathbf{R}_1^0, \ldots \mathbf{R}_N^0; T_{\rm el})$ denote the total free energy of the system when all atoms are fixed at their perfect-lattice positions $\mathbf{R}_I^0$, and write $U(\mathbf{R}_1, \ldots \mathbf{R}_N; T_{\rm el}) = F_{\rm perf}(T_{\rm el}) + U_{\rm vib}(\mathbf{R}_1, \ldots \mathbf{R}_N; T_{\rm el})$, which defines the vibrational energy $U_{\rm vib}$. Then it follows from eqn (1) that

$$F = F_{\rm perf} + F_{\rm vib} \; , \tag{2}$$

where the vibrational free energy $F_{\rm vib}$ is given by:

$$F_{\rm vib} = -k_{\rm B} T \ln \left\{ \frac{1}{\Lambda^{3N}} \int d\mathbf{R}_1 \ldots d\mathbf{R}_N \, \exp[-\beta U_{\rm vib}(\mathbf{R}_1, \ldots \mathbf{R}_N; T_{\rm el})] \right\} \; . \tag{3}$$

(Note that we now omit the factor $N!$ from the partition function, since every atom is assumed to be confined to its own lattice site.) The vibrational energy $U_{\rm vib}$ can be further separated into harmonic and anharmonic parts ($U_{\rm vib} = U_{\rm harm} + U_{\rm anharm}$), in terms of which we can define the harmonic vibrational free energy $F_{\rm harm}$:

$$F_{\rm harm} = -k_{\rm B} T \ln \left\{ \frac{1}{\Lambda^{3N}} \int d\mathbf{R}_1 \ldots d\mathbf{R}_N \, \exp[-\beta U_{\rm harm}(\mathbf{R}_1, \ldots \mathbf{R}_N; T_{\rm el})] \right\} \; , \tag{4}$$

with the anharmonic free energy being the remainder $F_{\rm anharm} = F_{\rm vib} - F_{\rm harm}$. The harmonic energy $U_{\rm harm}$ is defined in the obvious way:

$$U_{\rm harm} = \frac{1}{2} \sum_{I,J} \mathbf{u}_I \cdot (\nabla_I \nabla_J U) \cdot \mathbf{u}_J \; , \tag{5}$$

where $\mathbf{u}_I$ is the displacement of atom I from its perfect-lattice position ($\mathbf{u}_I \equiv \mathbf{R}_I - \mathbf{R}_I^0$) and the double gradient of the *ab initio* total energy is evaluated with all atoms at their perfect-lattice positions. Since we are dealing with a crystal, we shall usually prefer to rewrite $U_{\rm harm}$ in the more explicit form:

$$U_{\rm harm} = \frac{1}{2} \sum_{ls\alpha, l't\beta} u_{ls\alpha} \Phi_{ls\alpha, l't\beta} u_{l't\beta} \; , \tag{6}$$

where $u_{ls\alpha}$ is the αth Cartesian component of the displacement of atom number s in primitive cell number l, and $\Phi_{ls\alpha,l't\beta}$ is the force-constant matrix. It should be noted that the present separation of F does not represent a separation into electronic and nuclear contributions, since thermal electronic excitations influence all three parts of F.

Since all other thermodynamic functions can be obtained by taking appropriate derivatives of the Helmholtz free energy, the separation of F into components implies a similar separation of other quantities. For example, the pressure $p = -(\partial F / \partial V)_T$ is $p_{\rm perf} + p_{\rm harm} + p_{\rm anharm}$, where $p_{\rm perf} = -(\partial F_{\rm perf} / \partial V)_T$, and similarly for the components $p_{\rm harm}$ and $p_{\rm anharm}$.

C. Phonon frequencies

The free energy of a harmonic oscillator of frequency ω is $k_{\rm B} T \ln \left(\exp(\frac{1}{2}\beta\hbar\omega) - \exp(-\frac{1}{2}\beta\hbar\omega) \right)$, which has the high-temperature expansion $k_{\rm B} T \ln(\beta\hbar\omega) + k_{\rm B} T \left[\frac{1}{24}(\beta\hbar\omega)^2 + O((\beta\hbar\omega)^4) \right]$, so that the harmonic free energy per atom of the vibrating crystal in the classical limit is:

$$F_{\rm harm} = \frac{3 k_{\rm B} T}{N_{\mathbf{k}s}} \sum_{\mathbf{k}s} \ln(\beta\hbar\omega_{\mathbf{k}s}) \; , \tag{7}$$

where $\omega_{\mathbf{k}s}$ is the frequency of phonon branch s at wavevector $\mathbf{k}$ and the sum goes over the first Brillouin zone, with $N_{\mathbf{k}s}$ the total number of k-points and branches in the sum. It will be useful to express this in terms of the geometric average $\bar{\omega}$ of the phonon frequencies, defined as:

$$\ln \bar{\omega} = \frac{1}{N_{\mathbf{k}s}} \sum_{\mathbf{k}s} \ln(\omega_{\mathbf{k}s}) \; , \tag{8}$$

which allows us to write:

$$F_{\mathrm{harm}} = 3k_{\mathrm{B}}T\ln(\beta\hbar\bar{\omega}) \ . \tag{9}$$

The central quantity in the calculation of the frequencies is the force-constant matrix $\Phi_{ls\alpha,l't\beta}$, since the frequencies at wavevector $\mathbf{k}$ are the eigenvalues of the dynamical matrix $D_{s\alpha,t\beta}$, defined as:

$$D_{s\alpha,t\beta}(\mathbf{k}) = \frac{1}{M}\sum_{l'}\Phi_{ls\alpha,l't\beta}\exp\left[i\mathbf{k}\cdot(\mathbf{R}^0_{l't} - \mathbf{R}^0_{ls})\right] \ , \tag{10}$$

where $\mathbf{R}^0_{ls}$ is the perfect-lattice position of atom s in primitive cell number l. If we have the complete force-constant matrix, then $D_{s\alpha,t\beta}$ and hence the frequencies $\omega_{\mathbf{k}s}$ can be obtained at any $\mathbf{k}$, so that $\bar{\omega}$ can be computed to any required precision. In principle, the elements of $\Phi_{ls\alpha,l't\beta}$ are non-zero for arbitrarily large separations $\mid \mathbf{R}^0_{l't} - \mathbf{R}^0_{ls} \mid$, but in practice they decay rapidly with separation, so that a key issue in achieving our target precision is the cut-off distance beyond which the elements can be neglected.

We calculate $\Phi_{ls\alpha,l't\beta}$ by the small-displacement method, in a way similar to that described in Ref. [52]. The basic principle is that $\Phi_{ls\alpha,l't\beta}$ describes the proportionality between displacements and forces. If the atoms are given small displacements $u_{ls\alpha}$ from their perfect-lattice positions, then to linear order the forces $F_{ls\alpha}$ are:

$$F_{ls\alpha} = -\sum_{l't\beta}\Phi_{ls\alpha,l't\beta}u_{l't\beta} \ . \tag{11}$$

Within the *ab initio* scheme, all the elements $\Phi_{ls\alpha,l't\beta}$ are obtained for a given $l't\beta$ by introducing a small displacement $u_{l't\beta}$, all other displacements being zero, minimising the electronic free energy, and evaluating all the forces $F_{ls\alpha}$. In practice, the displacement amplitude $u_{l't\beta}$ must be made small enough to ensure linearity to the required precision, and this sets the precision with which the electronic free energy must be minimised.

By translational symmetry, the entire force-constant matrix is obtained by making three independent displacements for each atom in the primitive cell, and this means that no more than $3N_{\mathrm{bas}}$ calculations are needed, where N_{bas} is the number of atoms in the primitive cell. This number can be reduced by symmetry. If, as in the h.c.p. crystal, all atoms in the primitive cell are equivalent under operations of the space group, then the entire force-constant matrix can be obtained by making at most three displacements of a single atom in the primitive cell: from $\Phi_{ls\alpha,l't\beta}$ for one chosen atom $l't$, one obtains $\Phi_{ls\alpha,l't\beta}$ for all other $l't$. Point-group symmetry reduces the number still further if linearly independent displacements of the chosen atom are equivalent by symmetry. This is the case in the h.c.p. structure, since displacements in the basal plane related by rotations about the c-axis by $\pm 120°$ are equivalent by symmetry; this means that two calculations, one with the displacement along the c-axis, and other with the displacement in the basal plane, suffice to obtain the entire $\Phi_{ls\alpha,l't\beta}$ matrix. The basal-plane displacement should be made along a symmetry direction, because the symmetry makes the calculations more efficient. Since the exact $\Phi_{ls\alpha,l't\beta}$ matrix has point-group symmetries, the calculated $\Phi_{ls\alpha,l't\beta}$ must be symmetrised to ensure that these symmetries are respected. The symmetrisation also serves to eliminate the lowest-order non-linearities in the relation between forces and displacements [52].

It is important to appreciate that the $\Phi_{ls\alpha,l't\beta}$ in the formula for $D_{s\alpha,t\beta}(\mathbf{k})$ is the force-constant matrix in the infinite lattice, with no restriction on the wavevector $\mathbf{k}$, whereas the *ab initio* calculations of $\Phi_{ls\alpha,l't\beta}$ can only be done in supercell geometry. Without a further assumption, it is strictly impossible to extract the infinite-lattice $\Phi_{ls\alpha,l't\beta}$ from supercell calculations, since the latter deliver information only at wavevectors that are reciprocal lattice vectors of the superlattice. The further assumption needed is that the infinite-lattice $\Phi_{ls\alpha,l't\beta}$ vanishes when the separation $\mathbf{R}_{l't} - \mathbf{R}_{ls}$ is such that the positions $\mathbf{R}_{ls}$ and $\mathbf{R}_{l't}$ lie in different Wigner-Seitz (WS) cells of the chosen superlattice. More precisely, if we take the WS cell centred on $\mathbf{R}_{l't}$, then the infinite-lattice value of $\Phi_{ls\alpha,l't\beta}$ vanishes if $\mathbf{R}_{ls}$ is in a different WS cell; it is equal to the supercell value if $\mathbf{R}_{ls}$ is wholly within the same WS cell; and it is equal to the supercell value divided by an integer P if $\mathbf{R}_{ls}$ lies on the boundary of the same WS cell, where P is the number of WS cells having $\mathbf{R}_{ls}$ on their boundary. With this assumption, the $\Phi_{ls\alpha,l't\beta}$ elements will converge to the correct infinite-lattice values as the dimensions of the supercell are systematically increased.

D. Anharmonicity

1. Thermodynamic integration

Although we shall show that the anharmonic free energy F_{anharm} is numerically fairly small, it is far more challenging to calculate than F_{perf} or F_{harm}, because there is no simple formula like eqn (7), and the direct computation of the multi-dimensional integrals in the free-energy formulas such as eqn (4) is impossible. Instead, we use the technique of thermodynamic integration (see e.g. Ref. [53]) to obtain the difference $F_{\rm vib} - F_{\rm harm}$, as developed in earlier papers [2–4].

Thermodynamic integration is a completely general technique for determining the difference of free energies $F_1 - F_0$ for two systems whose total-energy functions are U_1 and U_0. The basic idea is that $F_1 - F_0$ represents the reversible work done on continuously and isothermally switching the energy function from U_0 to U_1. To do this switching, a continuously variable energy function U_λ is defined as:

$$U_\lambda = (1-\lambda) U_0 + \lambda U_1 \; , \tag{12}$$

so that the energy goes from U_0 to U_1 as λ goes from 0 to 1. In classical statistical mechanics, the work done in an infinitesimal change $d\lambda$ is:

$$dF = \langle dU_\lambda / d\lambda \rangle_\lambda d\lambda = \langle U_1 - U_0 \rangle_\lambda d\lambda \; , \tag{13}$$

where $\langle \cdot \rangle_\lambda$ represents the thermal average evaluated for the system governed by U_λ. It follows that:

$$F_1 - F_0 = \int_0^1 d\lambda \, \langle U_1 - U_0 \rangle_\lambda \; . \tag{14}$$

In practice, this formula can be applied by calculating $\langle U_1 - U_0 \rangle_\lambda$ for a suitable set of λ values and performing the integration numerically. The average $\langle U_1 - U_0 \rangle_\lambda$ is evaluated by sampling over configuration space.

For the anharmonic free energy, a possible approach is to choose U_0 as $U_{\rm harm}$ and U_1 as $U_{\rm vib}$, so that $F_1 - F_0$ is the anharmonic free energy $F_{\rm anharm}$. This was the procedure used in our earlier *ab initio* work on the melting of Al [3], and a related technique was used by Sugino and Car [2] in their work on Si melting. However, the calculations are rather heavy, and the need for extensive sampling over the electronic Brillouin zone in the *ab initio* calculations makes it difficult to achieve high precision. We have now developed a more efficient two-step procedure, in which we go first from the harmonic *ab initio* system $U_{\rm harm}$ to an intermediate reference system $U_{\rm ref}$ which closely mimics the full *ab initio* total energy $U_{\rm vib}$; in the second step, we go from $U_{\rm ref}$ to $U_{\rm vib}$. The anharmonic free energy is thus represented as:

$$F_{\rm anharm} = (F_{\rm vib} - F_{\rm ref}) + (F_{\rm ref} - F_{\rm harm}) \; , \tag{15}$$

and the two differences are calculated by separate thermodynamic integrations:

$$\begin{aligned} F_{\rm vib} - F_{\rm ref} &= \int_0^1 d\lambda \, \langle U_{\rm vib} - U_{\rm ref} \rangle_\lambda^{\rm vr} \\ F_{\rm ref} - F_{\rm harm} &= \int_0^1 d\lambda \, \langle U_{\rm ref} - U_{\rm harm} \rangle_\lambda^{\rm rh} \; . \end{aligned} \tag{16}$$

To distinguish clearly between these two parts of the calculation, we denote by $\langle \cdot \rangle_\lambda^{\rm rh}$ the thermal average taken in the ensemble generated by the switched total energy $U_\lambda^{\rm rh} \equiv (1-\lambda) U_{\rm harm} + \lambda U_{\rm ref}$ and by $\langle \cdot \rangle_\lambda^{\rm vr}$ the corresponding average for $U_\lambda^{\rm vr} \equiv (1-\lambda) U_{\rm ref} + \lambda U_{\rm vib}$.

The crucial point of this is that $U_{\rm ref}$ is required to consist of an empirical model potential which quite accurately represents both the harmonic and anharmonic parts of the *ab initio* total energy $U_{\rm vib}$. Since it is a model potential, the thermodynamic integration for $F_{\rm ref} - F_{\rm harm}$ can be performed with high precision on large systems. The difference $F_{\rm vib} - F_{\rm ref}$, by contrast, involves heavy *ab initio* calculations, but provided a good $U_{\rm ref}$ can be found these are manageable. We return to the problem of searching for a good $U_{\rm ref}$ in Sec. II D 3.

2. Calculation of thermal averages

The calculation of thermal averages is just the standard problem of computational statistical mechanics, and can be accomplished by any method that allows us to draw unbiased samples of configurations from the appropriate ensemble. In this work, we employ molecular dynamics simulation. This means, for example, that to calculate $\langle U_{\rm ref} - U_{\rm harm} \rangle_\lambda^{\rm rh}$ we generate a trajectory of the system using equations of motion derived from the total energy function $U_\lambda^{\rm rh}$. In the usual way, an initial part of the trajectory is discarded for equilibration, and the remainder is used to estimate the average. The duration of this remainder must suffice to deliver enough *independent* samples to achieve the required statistical precision.

The key technical problem in calculating thermal averages in nearly harmonic systems is that of ergodicity. In the dynamical evolution of a perfectly harmonic system, energy is never shared between different vibrational modes, so that a system starting at any point in phase space fails to explore the whole of phase space. This means that in a nearly harmonic system exploration will be very slow and inefficient, and it is difficult to generate statistically independent samples. We solve this following Ref. [3]: the statistical sampling is performed using Andersen molecular dynamics [54], in which the atomic velocities are periodically randomised by drawing them from a Maxwellian distribution. This type of simulation generates the canonical ensemble and completely overcomes the ergodicity problem.

3. Reference system

The computational effort needed to calculate $F_{\rm vib} - F_{\rm ref}$ is greatly reduced if the difference of total energies $U_{\rm vib} - U_{\rm ref}$ is small, for two reasons. First, the amount of sampling needed to calculate $\langle U_{\rm vib} - U_{\rm ref} \rangle_\lambda$ to a given precision is reduced if the fluctuations of $U_{\rm vib} - U_{\rm ref}$ are small; second, the variation of $\langle U_{\rm vib} - U_{\rm ref} \rangle_\lambda$ as λ goes from 0 to 1 is reduced. In fact, if the fluctuations are small enough, this variation can be neglected, and it is accurate enough to approximate $F_{\rm vib} - F_{\rm ref} \simeq \langle U_{\rm vib} - U_{\rm ref} \rangle_{\rm ref}$, with the average taken in the reference ensemble. If this is not good enough, the next approximation is readily shown to be:

$$F_{\rm vib} - F_{\rm ref} \simeq \langle U_{\rm vib} - U_{\rm ref} \rangle_{\rm ref} - \frac{1}{2 k_{\rm B} T} \left\langle [U_{\rm vib} - U_{\rm ref} - \langle U_{\rm vib} - U_{\rm ref} \rangle_{\rm ref} \rangle]^2 \right\rangle_{\rm ref} . \tag{17}$$

Our task is therefore to search for a model $U_{\rm ref}$ for which the fluctuations of $U_{\rm vib} - U_{\rm ref}$ are as small as possible.

The question of reference systems for Fe has already been discussed in our recent *ab initio* simulation work on the high-pressure liquid [32]. We showed there that a remarkably good reference model is provided by a system interacting through inverse-power pair potentials:

$$U_{\rm IP} = \frac{1}{2} \sum_{I \neq J} \phi(\mid \mathbf{R}_I - \mathbf{R}_J \mid) , \tag{18}$$

where $\phi(r) = B / r^\alpha$, with B and α adjusted to minimise the fluctuations of the difference between $U_{\rm IP}$ and the *ab initio* energy. Unfortunately, we shall show that this is an unsatisfactory reference model for the solid, because the harmonic phonon dispersion relations produced by $U_{\rm IP}$ differ markedly from the *ab initio* ones. It is a particularly poor reference model at low temperatures where anharmonic corrections are small, because in that régime a good reference system must closely resemble $U_{\rm harm}$. However, we find that $U_{\rm IP}$ becomes an increasingly good reference system as T approaches the melting temperature. We therefore adopt as a general form for the reference system a linear combination of $U_{\rm harm}$ and $U_{\rm IP}$:

$$U_{\rm ref} = c_1 U_{\rm harm} + c_2 U_{\rm IP} . \tag{19}$$

The coefficients c_1 and c_2 are adjusted to minimise the intensity of the fluctuations of $U_{\rm vib} - U_{\rm ref}$ for each thermodynamic state.

Now consider in more detail how this optimisation of $U_{\rm ref}$ is to be done. In principle, the ensemble in which we have to sample the fluctuations of $U_{\rm vib} - U_{\rm ref}$ is the one generated by the continuously switched total energy $(1 - \lambda) U_{\rm ref} + \lambda U_{\rm vib}$ that governs the thermodynamic integration from $U_{\rm ref}$ to $U_{\rm vib}$. In practice, this is essentially the same as sampling in either of the ensembles associated with $U_{\rm ref}$ or $U_{\rm vib}$, provided the fluctuations of $U_{\rm vib} - U_{\rm ref}$ are indeed small. But even this poses a problem. We are reluctant to sample in the ensemble of $U_{\rm vib}$, because extensive (and expensive) *ab initio* calculations are needed to achieve adequate statistical accuracy. On the other hand, we cannot sample in the ensemble of $U_{\rm ref}$ without knowing $U_{\rm ref}$, which is what we are trying to find. We resolve this problem by constructing an initial optimised $U_{\rm ref}$ by minimising the fluctuations in the ensemble of $U_{\rm harm}$. We then use this initial $U_{\rm ref}$ to generate a new set of samples, which is then used to reoptimise $U_{\rm ref}$. In principle, we should probably repeat this procedure until $U_{\rm ref}$ ceases to vary, but in practice we stop after the second iteration. Note that even this approach requires fully converged *ab initio* calculations for a large set of configurations. But since the configurations are generated with the potential model $U_{\rm ref}$, statistically independent samples are generated with much less effort than if we were using $U_{\rm vib}$ to generate them.

III. THE RIGID PERFECT LATTICE

Our DFT calculations on the rigid perfect lattice give $F_{\rm perf}$, and hence quantities such as electronic specific heat $C_{\rm perf}$ and the pressure $p_{\rm perf}$ for any chosen volume and electronic temperature $T_{\rm el}$. We do not discuss the low-temperature behaviour, since there have already been many DFT studies of this [27–29,32]. The various DFT calculations are in excellent accord, and reproduce accurately the low-temperature $p(V)$ relation measured in DAC experiments [9], especially at high pressures. The difference between the pressures calculated with the present PAW techniques and experimental values ranges from 4.5 % at 100 GPa to 2.5 % at 300 GPa, these deviations being only slightly greater than the scatter on the experimental values. Our results for the high-temperature thermodynamic properties of the rigid perfect lattice will be reported rather briefly, since they mainly confirm what is known in less detail from previous work [8,36].

All the calculations of this Section employ the $15 \times 15 \times 9$ electronic Monkhorst-Pack set, which gives 135 k-points in the irreducible wedge of the Brillouin zone. Tests with finer k-point sets show that the residual k-point errors are less than 1 meV/atom for $T \geq 2000$ K. We performed calculations of $F_{\rm perf}$ at a set of atomic volumes from 6.2 to 11.4 Å^3 at intervals of 0.2 Å^3, and for every volume for $T_{\rm el}$ going from 200 to 10,000 K at intervals of 200 K. The calculations also deliver the internal energy $E_{\rm perf}$ and the electronic entropy $S_{\rm perf}$, from which we obtain the specific heat either as $C_{\rm perf} = (\partial E_{\rm perf} / \partial T)_V$, or as $C_{\rm perf} = T(\partial S_{\rm perf}/\partial T)_V$ – consistency between the two methods provides a useful check.

Our results for $C_{\rm perf}$ are reported in Fig. 1 for the $T_{\rm el}$ range $0 - 6000$ K at four atomic volumes. As expected from previous work [8,36,55], $C_{\rm perf}$ becomes large at high temperatures, its value of *ca.* $2k_{\rm B}$ at 6000 K being comparable with the Dulong-Petit specific heat of lattice vibrations ($3k_{\rm B}$), so that thermal electronic excitations are crucial to a correct description of Fe thermodynamics at core conditions. Our $C_{\rm perf}$ results are numerically quite close to those reported by Wasserman *et al.* [36], though the latter actually refer to f.c.c. Fe. The linear dependence of $C_{\rm perf}$ on T evident in Fig. 1 at low T ($C_{\rm perf} = \gamma T + O(T^2)$) is expected from the standard Sommerfeld expansion [56] for electronic specific heat in powers of T, which shows that the low-temperature slope is given by $\gamma = \frac{1}{3}\pi^2 k_{\rm B}^2 g(E_{\rm F})$, where $g(E_{\rm F})$ is the electronic density of states (DOS, i.e. the number of states per unit energy per atom) at the Fermi energy $E_{\rm F}$. We have made separate calculations of the DOS and obtained γ from $g(E_{\rm F})$, which give a useful cross-check on the low-temperature slope of $C_{\rm perf}$.

In order to obtain other thermodynamic functions, we need a fit to our $F_{\rm perf}$ results. At each temperature, we fit the results to the standard Birch-Murnaghan form, using exactly the procedure followed in our recent work on the Fe/O system [35]. This involves fitting the 22 values of $F_{\rm perf}$ at a given temperature using four fitting parameters (E_0, V_0, K and K' in the notation of Ref. [35]). We find that at all temperatures the r.m.s. fitting errors are less than 1 meV at all points. The temperature variation of the fitting parameters is then represented using a polynomial of sixth degree.

Electronic excitations have a significant effect on the pressure, as can be seen by examining the T-dependence of the perfect-lattice pressure $p_{\rm perf} = -(\partial F_{\rm perf}/\partial V)_T$. We display in Fig. 2 the thermal part $\Delta p_{\rm perf}$ of $p_{\rm perf}$, i.e. the difference between $p_{\rm perf}$ at a given T and its zero-temperature value. The thermal excitation of electrons produces a positive pressure. This is what intuition would suggest, but it is worth noting the reason. Since $F_{\rm perf}(T_{\rm el}) = F_{\rm perf}(0) - \frac{1}{2}T^2\gamma(V)$ at low temperatures, the change of pressure due to electronic excitations is $\Delta p = \frac{1}{2}T^2 d\gamma/dV$ in this region. But $d\gamma/dV > 0$, so that the electronic thermal pressure must be positive. To put the magnitude of this pressure in context, we recall that at the Earth's inner-core boundary (ICB) the pressure is 330 GPa and the temperature is believed to be in the range $5000 - 6000$ K, the atomic volume of Fe under these conditions being *ca.* 7 Å^3. Our results then imply that electronic thermal pressure accounts for *ca.* 4 % of the total pressure, which is small but significant.

IV. THE HARMONIC CRYSTAL

A. Convergence tests

We have made extensive tests to ensure that our target precision of 10 meV/atom is attained for the harmonic free energy $F_{\rm harm}$. We note that at 6000 K this requires that the geometric mean frequency $\bar{\omega}$ be calculated with a precision of 0.7 %. Convergence of $\bar{\omega}$ must be achieved with respect to four main parameters: the atomic displacement used to calculate the force-constant matrix $\Phi_{ls\alpha,l't\beta}$; the electronic k-point sampling; the size of the repeating cell used to obtain $\Phi_{ls\alpha,l't\beta}$; and the density of the k-point mesh used in calculating $\bar{\omega}$ from $\omega_{\mathbf{k}s}$ by integration over the phonon Brillouin zone (see eqn(7)).

The technical measures taken to achieve convergence are as follows. Integration over the phonon Brillouin zone was performed using 364 Monkhorst-Pack k-points in the irreducible wedge, and an atomic displacement amplitude of 0.0148 Å was used; the associated errors in $F_{\rm harm}$ are less than 1 meV/atom in both cases. For electronic k-point sampling, we use the $5 \times 5 \times 5$ Monkhorst-Pack set, which reduces k-point errors to less than 0.1 meV/atom at all temperatures $T_{\rm el}$ of interest. Finally, we tested the convergence of $F_{\rm harm}$ with respect to the size of repeating cell used to generate $\Phi_{ls\alpha,l't\beta}$, going up to cells containing 150 atoms. We found that with the $3 \times 3 \times 2$ repeating cell the error in $F_{\rm harm}$ calculated at the atomic volume $V = 8.67$ Å and $T = 4300$ K is a little over 2 meV/atom, and we adopted this cell size for all the calculations.

B. Dispersion relations, average frequency, free energy

In Fig. 3 we present the harmonic phonon dispersion relations at the two atomic volumes 8.67 and 6.97 Å^3 calculated with $T_{\rm el} = 4000$ K. We are not aware of previous direct *ab initio* calculations of the phonon frequencies of high-pressure h.c.p. Fe, but there are published dispersion relations derived from a 'generalised pseudopotential' parameterisation of FP-LMTO calculations performed by Söderlind *et al.* [28] using the LDA at the atomic volume 6.82 Å^3. The agreement of their phonon frequencies with ours is far from perfect. For example, we find that the maximum frequency in the Brillouin zone calculated at $V = 6.82$ Å^3 is at the Γ-point and is 21.2 THz, whereas they find the maximum frequency at the M-point with the value 17.2 THz. This is not unexpected, since they report that the generalised pseudopotential scheme fails to reproduce accurately some phonon frequencies calculated directly with FP-LMTO in the f.c.c. Fe crystal [28]; in addition, the LDA used by them is known to underestimate phonon frequencies in Fe [29].

Casual inspection suggests that our dispersion curves at the two atomic volumes are almost identical apart from an overall scale factor. This suggestion can be judged from the right-hand panel of Fig. 3, where we plot as dashed curves the dispersion curves at $V = 8.67$ Å^3 scaled by the factor 1.409 – the reason for choosing this factor will be explained below. The comparison shows that the curves at the two volumes are indeed related by a single scaling factor to within *ca.* 5 %. We also take the opportunity here to check how well the inverse-power potential model $U_{\rm IP}$ (see Eqn (18)) reproduces phonon frequencies. To do this, we take exactly the same parameters B and α specifying $\phi(r)$ that reproduced well the properties of the liquid [32], namely $\alpha = 5.86$ and B such that for $r = 2.0$ Å $\phi(r) = 1.95$ eV. The phonons calculated from this model are compared with the *ab initio* phonons at atomic volume $V = 8.67$ Å in the left panel of Fig. 3. Although the general form of the dispersion curves is correctly reproduced, it is clear that the model gives only a very rough description, with discrepancies of as much as 30 % for some frequencies.

We performed direct *ab initio* calculations of the dispersion relations and hence the geometric mean frequency $\bar{\omega}$ for seven volumes spaced roughly equally from 9.72 to 6.39 Å^3, and for each of these volumes for $T_{\rm el}$ from 1000 to 10,000 K at intervals of 500 K. The results for $\bar{\omega}$ as function of volume are reported in Fig. 4 for the three temperatures $T_{el} = 2000$, 4000 and 6000 K. We use a (natural) log-log plot to display the results, so that the negative slope $\gamma_{\rm ph} \equiv -d \ln \bar{\omega} / d \ln V$ is the so-called phonon Grüneisen parameter. (The relation between $\gamma_{\rm th}$ and the thermodynamic Grüneisen parameter γ will be discussed in Sec. VI B.) We note that if phonon dispersion curves at two different volumes are related by a simple scaling factor, this must be the ratio of $\bar{\omega}$ values at the two volumes. The scaling factor used in Fig. 3 was obtained in exactly this way from our $\bar{\omega}$ results. The Grüneisen parameter $\gamma_{\rm ph}$ increases with increasing volume, in accord with a widely used rule of thumb [57]. We find that $\gamma_{\rm ph}$ goes from 1.34 at $V = 6.7$ Å^3 to 1.70 at $V = 8.3$ Å^3, but then decreases slightly to 1.62 at $V = 9.5$ Å^3. Fig. 3 also allows us to judge the effect of $T_{\rm el}$ on phonon frequencies: for all volumes studied, the frequencies decrease by *ca.* 4 % as $T_{\rm el}$ goes from 2000 to 6000 K. However, we mention that for the higher volumes, though not for the smaller ones, $\bar{\omega}$ slightly increases again as $T_{\rm el}$ goes to still higher values. To enable the $\bar{\omega}$ data to be used in thermodynamic calculations, we parameterise the temperature dependence of $\ln \bar{\omega}$ at each volume as $a + bT^2 + cT^3 + eT^5$, and the volume dependence of the four coefficients a, b, c and e as a third-degree polynomial in V.

We now return to the matter of quantum nuclear corrections. Since the leading high-temperature correction to the free energy is $\frac{1}{24} k_{\rm B} T (\beta \hbar \omega)^2$ per mode and there are three modes per atom, the quantum correction to $F_{\rm harm}$ is $\frac{1}{8} k_{\rm B} T (\beta \hbar \langle \omega^2 \rangle^{1/2})^2$ per atom, where $\langle \omega^2 \rangle$ denotes the average of ω^2 over wavevectors and branches. At the lowest volume of interest, $V = 7$ Å^3, $\langle \omega^2 \rangle^{1/2} / 2\pi$ is roughly 15 THz. At the lowest temperature of interest, $T = 2000$ K, this gives a quantum correction of 3 meV/atom, which is small compared with our target precision.

C. Harmonic phonon specific heat and thermal pressure

If the mean frequency $\bar{\omega}$ were independent of temperature, the constant-volume specific heat $C_{\rm harm}$ due to harmonic phonons would be exactly $3k_{\rm B}$ per atom in the classical limit employed here. We find that its temperature dependence yields a slight increase of $C_{\rm harm}$ above this value, but this is never greater than $0.25k_{\rm B}$ under the conditions of interest. The harmonic phonon pressure $p_{\rm harm}$ as a function of atomic volume at different temperatures is reported in Fig. 5. Comparison with Fig. 2 shows that $p_{\rm harm}$ is always much bigger (by a factor of at least three) than the electronic thermal pressure under the conditions of interest. At ICB conditions ($p = 330$ GPa, $T \sim 5000 - 6000$ K), $p_{\rm harm}$ account for *ca.* 15 % of the total pressure.

V. ANHARMONIC FREE ENERGY

A. Optimisation of reference system

It was stressed in Sec. II D 3 that optimisation of the reference system greatly improves the efficiency of the anharmonic calculations. We investigated the construction of the reference system in detail at the atomic volume 8.67 Å^3, with the optimisations performed for a simulated system of 16 atoms. The calculation of the anharmonic free energy itself for a system as small as this would not be adequate, but we expect this system size to suffice for the optimisation of $U_{\rm ref}$. The initial sample of configurations (see Sec. II D 3) was taken from a simulation of duration 100 ps performed with the total energy $U_{\rm harm}$, with velocity randomisation typically every 0.2 ps. Configurations were taken every 1 ps, so that we obtain a sample of 100 configurations. In computing the energy difference $U_{\rm vib} - U_{\rm ref}$ for these configurations, the *ab initio* energy $U_{\rm vib}$ was always computed using $5 \times 5 \times 3$ Monkhorst-Pack electronic k-point sampling (38 k-points in the full Brillouin zone). Once the preliminary optimisation had been performed with configurations generated like this, the resulting $U_{\rm ref}$ was used to produce a new set of 100 configurations with an Andersen MD simulation of the same duration as before, and the reference system was reoptimised.

This entire procedure was carried out at temperatures of 1000 and 4000 K. The values of the optimisation coefficients (see Eqn (19)) were $c_1 = 0.2$, $c_2 = 0.8$ at the high temperature and $c_1 = 0.7$, $c_2 = 0.3$ at the low temperature. (We do not require that $c_1 + c_2 = 1$, though this happens to be the case here.) As expected, $U_{\rm ref}$ resembles $U_{\rm harm}$ quite closely at the low temperature and $U_{\rm IP}$ quite closely at the high temperature.

In view of the labour involved in the optimisation, we wanted to find out whether the detailed choice of c_1 and c_2 makes a large difference to the strength of the fluctuations of $U_{\rm vib} - U_{\rm ref}$. To do this, we computed these fluctuations at several temperatures, using the two reference models just described, i.e. without optimising the c_i coefficients at each temperature. Our conclusion is that the values $c_1 = 0.2$, $c_2 = 0.8$ can safely be used at all the state points of interest, without incurring large fluctuations, and we therefore used this way of making the reference system in all subsequent calculations.

B. From harmonic *ab initio* to reference to full *ab initio*

The thermodynamic integration from *ab initio* harmonic to reference was done with nine equally-spaced λ-points using Simpson's rule, which gives an integration precision well in excess of our target. To investigate the influence of system size, integration from $U_{\rm harm}$ to $U_{\rm ref}$ was performed for systems of 12 different sizes, going from 16 to 1200 atoms. The calculations were also repeated with the force-constant matrix in $U_{\rm harm}$ generated with cells containing from 16 to 150 atoms (see Sec. II C). These tests showed that if the thermodynamic integration is done with a system of 288 atoms and the force constant used for $U_{\rm harm}$ is generated with the 36-atom cell, then the resulting difference $F_{\rm ref} - F_{\rm harm}$ is converged to better than 3 meV/atom.

To compute the difference $F_{\rm vib} - F_{\rm ref}$, we used the second-order expansion formula given in Eqn (17). Given the small size of the fluctuations of $U_{\rm vib} - U_{\rm ref}$, we expect this to be very accurate. The calculations of $F_{\rm vib} - F_{\rm ref}$ were all done with the 16-atom system. Tests with 36- and 64-atom systems show that this free-energy difference is converged with respect to size effects to within *ca.* 2 meV.

In classical statistical mechanics, $F_{\rm anharm}$ is expected to go as T^2 at low temperatures, and in fact we find that our results for $F_{\rm anharm}$ are well represented by $F_{\rm anharm} = a(V)T^2$ for all the temperatures studied. The volume dependence of $a(V)$ is adequately represented by $a(V) = \alpha_1 + \alpha_2 V$, with $\alpha_1 = 2.2\times10^{-9}$ eV K^{-2} and $\alpha_2 = -6.0\times10^{-10}$ eV Å^{-3} K^{-2} per atom. This means that for the atomic volumes of interest the anharmonic free energy is always negative, so that anharmonicity stabilises the solid. The temperature at which anharmonicity becomes appreciable is higher for smaller atomic volumes.

C. Anharmonic specific heat and pressure

Within the parameterisation just described, the anharmonic contribution to the constant-volume specific heat $C_{\rm anharm}$ is proportional to T and varies linearly with V. As an indication of its general size, we note that $C_{\rm anharm}$ increases from 0.09 to 0.18 $k_{\rm B}$ at 2000 K and from 0.28 to 0.53 $k_{\rm B}$ at 6000 K as V goes from 7 to 10 Å^3. The anharmonic contribution to the pressure is independent of volume, and is proportional to T^2. It increases from 0.4 to 3.5 GPa as T goes from 2000 to 6000 K, so that even at high temperatures it is barely significant.

VI. THERMODYNAMICS OF THE SOLID

We now combine the parameterised forms for $F_{\rm perf}$, $F_{\rm harm}$ and $F_{\rm anharm}$ presented in the previous three Sections to obtain the total free energy of the h.c.p. crystal, and hence, by taking appropriate derivatives, a range of other thermodynamic functions, starting with those measured in shock experiments.

A. Thermodynamics on the Hugoniot

In a shock experiment, conservation of mass, momentum and energy require that the pressure $p_{\rm H}$, the molar internal energy $E_{\rm H}$ and the molar volume $V_{\rm H}$ in the compression wave are related by the Rankine-Hugoniot formula [59]:

$$\frac{1}{2} p_{\rm H} (V_0 - V_{\rm H}) = E_{\rm H} - E_0 \; , \tag{20}$$

where E_0 and V_0 are the internal energy and volume in the zero-pressure state before the arrival of the wave. The quantities directly measured are the shock-wave and material velocities, which allow the values of $p_{\rm H}$ and $V_{\rm H}$ to be deduced. From a series of experiments, $p_{\rm H}$ as a function of $V_{\rm H}$ (the so-called Hugoniot) can be derived. The measurement of temperature in shock experiments is attempted but problematic [22].

The Hugoniot curve $p_{\rm H}(V_{\rm H})$ is straightforward to compute from our results: for a given $V_{\rm H}$, one seeks the temperature at which the Rankine-Hugoniot relation is satisfied; from this, one obtains $p_{\rm H}$ (and, if required, $E_{\rm H}$). In experiments on Fe, V_0 and E_0 refer to the zero-pressure b.c.c. crystal, and we obtain their values directly from GGA calculations, using exactly the same PAW technique and GGA as in the rest of the calculations. Since b.c.c. Fe is ferromagnetic, spin polarisation must be included, and this is treated by spin interpolation of the correlation energy due to Vosko *et al.* [58], as described in Refs. [32,41]. The value of E_0 includes the harmonic vibrational energy at 300 K, calculated from *ab initio* phonon dispersion relations for ferromagnetic b.c.c. Fe.

Our *ab initio* Hugoniot is compared with the measurements of Brown and McQueen [21] in Fig. 6. The agreement is good, with discrepancies ranging from 10 GPa at $V = 7.8$ Å^3 to 12 GPa at $V = 8.6$ Å^3. These discrepancies are only slightly greater than those found for the room-temperature static $p(V)$ curve (see Sec. III), which can be regarded as giving an indication of the intrinsic accuracy of the GGA itself. Another way of looking at the accuracy to be expected of the GGA is to recalculate the Hugoniot using the experimental value of the b.c.c. V_0 (11.8 Å^3, compared with the *ab initio* value of 11.55 Å^3). The Hugoniot calculated in this way is also plotted in Fig. 6, and we see that this gives almost perfect agreement with the experimental data in the pressure range $100 - 240$ GPa. We deduce from this that the *ab initio* Hugoniot deviates from the experimental data by an amount which should be expected from the known inaccuracies of the GGA applied to Fe. A similar comparison with the experimental Hugoniot was given in the tight-binding total-energy work of Wasserman *et al.* [36], and their agreement was as good as ours. We discuss the significance of this later.

Our Hugoniot temperature as a function of pressure is compared with the estimates of Brown and McQueen [21] and the experimental results of Yoo *et al.* [22] in Fig. 7. The *ab initio* temperatures agree well with those of Brown and McQueen, but fall substantially below those of Yoo *et al.*, and this supports the suggestion of Ref. [36] that the Yoo *et al.* measurements overestimate the Hugoniot temperature by *ca.* 1000 K.

A further quantity that can be extracted from shock experiments is the bulk sound velocity $v_{\rm B}$ as a function of atomic volume on the Hugoniot, which is given by $v_{\rm B} = (K_S/\rho)^{1/2}$, with $K_S \equiv -V(\partial p/\partial V)_S$ the adiabatic bulk modulus and ρ the mass density. Since K_S can be calculated from our *ab initio* pressure and entropy as functions of V and T, our calculated K_S can be directly compared with experimental values (Fig. 8). Here, there is a greater discrepancy than one would wish, with the theoretical values falling significantly above the K_S values of both Refs [21] and [20], although we note that the two sets of experimental results disagree by an amount comparable with the discrepancy between theory and experiment.

For what it is worth, we show in Fig. 9 a comparison between our calculated thermal expansivity on the Hugoniot with values extracted from shock data by Jeanloz [20]. The latter are very scattered, but is clear that the theoretical values have similar magnitude. However, our values vary little along the Hugoniot, whereas the experimental values seem to decrease rather rapidly with increasing pressure.

B. Other thermodynamic quantities

We conclude our presentation of results by reporting our *ab initio* predictions of quantities which characterise h.c.p. Fe at high pressures and temperatures, and allow some further comparisons with the predictions of Refs [8] and [36]. Our results are presented as a function of pressure on isotherms at $T = 2000$, 4000 and 6000 K. At each temperature, we give results only for the pressure range where, according to our *ab initio* melting curve [43], the h.c.p. phase is thermodynamically stable. In comparing with the predictions of Refs. [8,36], we use the explicit numerical results from Ref. [36] for thermodynamic quantities on the 2000 K isotherm. For the higher temperatures, we rely on the approximate parameterised formulas given in Ref. [8].

The total constant-volume specific heat per atom C_v (Fig. 10) emphasises again the importance of electronic excitations. In a purely harmonic system, C_v would be equal to $3k_{\rm B}$, and it is striking that C_v is considerably greater than that even at the modest temperature of 2000 K, while at 6000 K it is nearly doubled. The decrease of C_v with increasing pressure evident in Fig. 10 comes from the suppression of electronic excitations by high compression, and to a smaller extent from the suppression of anharmonicity. We note that our C_v values are significantly higher than those of Refs. [8,36]; the main reason for this seems to be our inclusion of anharmonic corrections and the T-dependence of harmonic frequencies [60].

The thermal expansivity α (Fig. 11) is one of the few cases where we can compare with DAC measurements [10]. The latter show that α decreases strongly with increasing pressure and our *ab initio* results fully confirm this. Our results also show that α increases significantly with temperature. Both trends are also shown by the calculations of Refs. [8,36], though the latter differ from ours in showing considerably larger values of α at low pressure and temperature.

The product αK_T of expansivity and isothermal bulk modulus is important because it is sometimes assumed to be independent of pressure and temperature over a wide range of conditions, and this constancy is used to extrapolate experimental data. Our predicted isotherms for αK_T (Fig. 12) indicate that its dependence on p is indeed weak, especially at low temperatures, but that its dependence on T certainly cannot be ignored, since it increases by at least 30 % as T goes from 2000 to 6000 K at high pressures. Wasserman *et al.* [36] come to qualitatively similar conclusions, and they also find values of *ca.* 10 MPa K^{-1} at $T \simeq 2000$ K. However, it is disturbing to note that the general tendency in our results for αK_T to increase with pressure at low pressures is not found in the results of Ref. [36] at 2000 K. In particular, they found a marked increase of αK_T with decreasing p, which does not occur in our results.

The thermodynamic Grüneisen parameter $\gamma \equiv V(\partial p/\partial E)_V \equiv \alpha K_T V/C_v$ plays an important role in high-pressure physics, because it relates the thermal pressure (i.e. the difference $p_{\rm th}$ between p at given V and T and p at the same V but $T = 0$) and the thermal energy (difference $E_{\rm th}$ between E at given V and T and E at the same V but $T = 0$). Assumptions about the value of γ are frequently used in reducing shock data from Hugoniot to isotherm. If one assumes that γ depends only on V, then the thermal pressure and energy are related by:

$$p_{\rm th} V = \gamma E_{\rm th} \ , \tag{21}$$

a relation known as the Mie-Grüneisen equation of state. At low temperatures, where only harmonic phonons contribute to $E_{\rm th}$ and $p_{\rm th}$, γ should indeed be temperature independent above the Debye temperature, because $E_{\rm th} = 3k_{\rm B}T$ per atom, and $p_{\rm th} V = -3k_{\rm B}T d\ln\bar{\omega}/d\ln V = 3k_{\rm B}T\gamma_{\rm th}$, so that $\gamma = \gamma_{\rm ph}$, which depends only on V. But in high-temperature Fe, the temperature independence of γ will clearly fail, because of electronic excitations (and anharmonicity).

Our results for γ (Fig. 13) indicate that it varies rather little with either pressure or temperature in the region of interest. At temperatures below *ca.* 4000 K, it decreases with increasing pressure, as expected from the behaviour of the phonon Grüneisen parameter $\gamma_{\rm ph}$ (see Sec. IV B). This is also expected from the often-used empirical rule of thumb [57] $\gamma \simeq (V/V_0)^q$, where V_0 is a reference volume and q is a constant exponent usually taken to be roughly unity. Since V decreases by a factor of about 0.82 as p goes from 100 to 300 GPa, this empirical relation would make γ decrease by the same factor over this range, which is roughly what we see. However, the pressure dependence of γ is very much weakened as T increases, until at 6000 K γ is almost constant. Our results agree moderately well with those of Refs. [8,36] in giving a value $\gamma \simeq 1.5$ at high pressures, but at low pressures there is a serious disagreement, since they find a strong increase of γ to values of over 2.0 as $p \to 0$, whereas our values never exceed 1.6.

VII. DISCUSSION AND CONCLUSIONS

Our primary interest in this work is in the properties of h.c.p. iron at high pressures and temperatures, but in order to investigate them using *ab initio* methods we have needed to make technical developments, which have a wider significance. The major technical achievement is that we have been able to calculate the *ab initio* free energy and other thermodynamic properties with completely controlled statistical-mechanical errors, i.e. errors that can be reduced to any required extent. Anharmonicity and thermal electronic excitations are fully included. The attainment of high precision for the electronic and harmonic parts of the free energy has required no particular technical innovations, though careful attention to sources of error is essential. The main innovation is in the development of well optimised reference systems for use with thermodynamic integration in the calculation of the anharmonic part, without which adequate precision would be impossible. With the methods we have developed, it becomes unnecessary to approximate the electronic structure with semi-empirical representations, or to resort to the statistical-mechanical approximations that have been used in the past.

We have assessed in detail the precision achieved in the various parts of the free energy. There are two kinds of errors: those incurred in the calculation of the free energies themselves, and those produced by fitting the results to polynomials. We have seen that the errors in calculating the perfect-lattice free energy F_{perf} are completely negligible, though there may be small fitting errors of perhaps 1 meV/atom. In the harmonic part F_{harm}, the calculational errors are *ca.* 3 meV/atom, most of which comes from spatial truncation of the force-constant matrix; the fitting error for F_{harm} are of about the same size. The most serious errors are in the anharmonic part F_{anharm}, and these are *ca.* 5 meV/atom in the calculation and *ca.* 4 meV/atom in the fitting. The overall technical errors therefore amount to *ca.* 15 meV/atom, which is slightly larger than our target of 10 meV/atom.

We stress that the precision just quoted does not take into account errors incurred in the particular implementation of DFT (PAW in the present work), for example the error associated with the chosen split between valence and core states. Such errors can in principle be systematically reduced, but we have not attempted this here. Nor does it account for the inaccuracy of the chosen E_{xc}, or for the neglect of the temperature dependence of E_{xc}. We shall attempt to assess errors of this type in a separate paper on the melting properties of Fe.

The most direct way to test the reliability of our methods is comparison with shock data for $p(V)$ on the Hugoniot [21], so it is gratifying to find close agreement over the pressure range of interest. The closeness of this agreement is inherently limited by the known inaccuracies of the GGA employed, and we have shown that the discrepancies are of the expected size. An important prediction of the calculations is the temperature $T(p)$ on the Hugoniot, since temperature is notoriously difficult to obtain in shock experiments. Our results support the reliability of the shock temperatures estimated by Brown and McQueen [21,62], and, in agreement with Wasserman *et al.* [36], we find that the temperatures of Yoo *et al.* [22] are too high by as much as 1000 K. This incidentally lends support to the reliability of the Brown and McQueen estimate of *ca.* 5500 K for the melting temperature of Fe at 243 GPa. The situation is not so satisfactory for the adiabatic bulk modulus K_S on the Hugoniot, since our *ab initio* values seem to be *ca.* 8 % above the shock values. But it should be remembered that even at ambient conditions *ab initio* and experimental bulk moduli frequently differ by this amount. The difficulties may be partly on the experimental side, since even for b.c.c. Fe at ambient conditions, experimental K_S values span a range of 8 %.

Our calculations fully confirm the strong influence of electronic thermal excitations [36,55]. At the temperatures $T \sim 6000$ K of interest for the Earth's core, their contribution to the specific heat is almost as large as that due to lattice vibrations, in line with previous estimates. They also have a significant effect on the Grüneisen parameter γ, which plays a key role in the thermodynamics of the core, and is poorly constrained by experiment. Our finding that γ decreases with increasing pressure for $T < 4000$ K accords with an often-used rule of thumb [57], but electronic excitations completely change this behaviour at core temperatures $T \sim 6000$ K, where γ has almost constant values of *ca.* 1.45, in accord with experimental estimates in the range 1.1 to 1.6 [21,63]. Comparison with the earlier tight-binding calculations of Wasserman *et al.* [36] both for γ and for the quantity αK_T is rather disquieting. We find two kinds of disagreement at low temperatures. First, they find an increase of αK_T as $p \to 0$, whereas we find the opposite. Even more seriously, their strong increase of γ as $p \to 0$ is completely absent in our results. Our calculations are more rigorous than theirs, since we completely avoid their statistical-mechanical approximations, as well as being fully self-consistent on the electronic-structure side. The suggestion must be that their approximations lead to significantly erroneous behaviour at low pressures.

The present work forms part of a larger project on both pure Fe and its alloys with S, O, Si and H in the solid and liquid states. In a separate paper, we shall demonstrate that the thermodynamic integration technique employed here can also be used to obtain the fully *ab initio* free energy and other thermodynamic functions of liquid Fe over a wide range of states, with a precision equal to what has been achieved here for the solid. From the free energies of solid and liquid, we are then able to determine the *ab initio* melting curve and the entropy and volume of fusion as functions of pressure [43].

In summary, we have presented extensive *ab initio* calculations of the free energy and a range of other thermodynamic properties of iron at high pressures and temperatures, in which all statistical-mechanical errors are fully under control, and a high (and quantified) precision has been achieved. We find close agreement with the most reliable shock data. *Ab initio* values are provided for important, but experimentally poorly determined quantities, such as the Grüneisen parameter. The free energy results provide part of the basis for the *ab initio* determination of the high-pressure melting properties of iron, to be reported in detail elsewhere.

ACKNOWLEDGMENTS

The work of DA is supported by NERC grant GST/02/1454 to G. D. Price and M. J. Gillan. We thank NERC and EPSRC for allocations of time on the Cray T3E machines at Edinburgh Parallel Computer Centre and Manchester CSAR service, these allocations being provided through the Minerals Physics Consortium (GST/02/1002) and the UK Car-Parrinello Consortium (GR/M01753). We gratefully acknowledge discussions with Prof. J.-P. Poirier and Dr. L. Vočadlo, and helpful comments on the original version of the manuscript by Prof. R. E. Cohen.

---

[1] L. Stixrude, R. E. Cohen and R. J. Hemley, Rev. Mineralogy **37**, 639 (1998).
[2] O. Sugino and R. Car, Phys. Rev. Lett. **74**, 1823 (1995).
[3] G. A. de Wijs, G. Kresse and M. J. Gillan, Phys. Rev. B **57**, 8223 (1998).
[4] D. Alfè, G. A. de Wijs, G. Kresse and M. J. Gillan, Int. J. Quant. Chem., in press.
[5] J.-P. Poirier, *Introduction to the Physics of the Earth's Interior*, Cambridge University Press, Cambridge (1991).
[6] J.-P. Poirier, Phys. Earth Planet. Inter. **85**, 319 (1994).
[7] T. G. Masters and P. M. Shearer, J. Geophys. Res. **95**, 21691 (1990).
[8] L. Stixrude, E. Wasserman and R. E. Cohen, J. Geophys. Res. **102**, 24729 (1997).
[9] H. K. Mao, Y. Wu, L. C. Chen, J. F. Shu and A. P. Jephcoat, J. Geophys. Res. **95**, 21737 (1990).
[10] R. Boehler, N. von Bargen and A. Chopelas, J. Geophys. Res. **95**, 731 (1990).
[11] R. Boehler, Nature **363**, 534 (1993).
[12] S. K. Saxena, G. Shen and P, Lazor, Science **260**, 1312 (1993).
[13] S. K. Saxena, G. Shen and P. Lazor, Science **264**, 405 (1994).
[14] S. K. Saxena, L. S. Dubrovinsky, P. Häggkvist, Y. Cerenius, G. Shen and H. K. Mao, Science **269**, 1703 (1995).
[15] S. K. Saxena, L. S. Dubrovinsky and P. Häggkvist, Geophys. Res. Lett. **23**, 2441 (1996).
[16] A. P. Jephcoat and S. P. Besedin, Phil. Trans. Roy. Soc. Series A **354**, 1333 (1996).
[17] D. Andrault, G. Fiquet, M. Kunz, F. Visocekas and D. Häusermann, Science **278**, 831 (1997).
[18] G. Shen, H. Mao, R. J. Hemley, T. S. Duffy and M. L. Rivers, Geophys. Res. Lett. **25**, 373 (1998).
[19] L. Vočadlo, J. Brodholt, D. Alfè, M. J. Gillan and G. D. Price, Phys. Earth Planet. Inter. **117**, 123 (2000).
[20] R. Jeanloz, J. Geophys. Res. **84**, 6059 (1979).
[21] J. M. Brown and R. G. McQueen, J. Geophys. Res. **91**, 7485 (1986).
[22] C. S. Yoo, N. C. Holmes, M. Ross, D. J. Webb and C. Pike, Phys. Rev. Lett. **70**, 3931 (1993).
[23] M. Matsui and O. L. Anderson, Phys. Earth Planet. Inter. **103**, 55 (1997).
[24] A. B. Belonoshko and R. Ahuja, Phys. Earth Planet. Inter. **102**, 171 (1997).
[25] P. Hohenberg and W. Kohn, Phys. Rev. **136**, B864 (1964); W. Kohn and L. Sham, Phys. Rev. A1133 (1965); R. O. Jones and O. Gunnarsson, Rev. Mod. Phys. **61**, 689 (1989); M. J. Gillan, Contemp. Phys. **38**, 115 (1997).
[26] C. S. Wang, B. M. Klein and H. Krakauer, Phys. Rev. Lett. **54**, 1852 (1985).
[27] L. Stixrude, R. E. Cohen and D. J. Singh, Phys. Rev. B **50**, 6442 (1994).

[28] P. Söderlind, J. A. Moriarty and J. M. Willis, Phys. Rev. B **53**, 14063 (1996).
[29] L. Vočadlo, G. A. de Wijs, G. Kresse, M. J. Gillan and G. D. Price, Faraday Disc. **106**, 205 (1997).
[30] H. K. Mao, J. Xu, V. V. Struzhkin, J. Shu, R. J. Hemley, W. Sturhahn, M. Y. Hu, E. E. Alp, L. Vočadlo, D. Alfè, G. D. Price, M. J. Gillan, M. Schwoerer-Böhning, D. Häsermann, P. Eng, G. Shen, H. Giefers, R. Lübbers, and G. Wortmann, Phys. Rev. Lett., submitted.
[31] G. A. de Wijs, G. Kresse, L. Vočadlo, D. Dobson, D. Alfè, M. J. Gillan and G. D. Price, Nature **392**, 805 (1998).
[32] D. Alfè, G. Kresse and M. J. Gillan, Phys. Rev. B, **61**, 132 (2000).
[33] D. Alfè and M. J. Gillan, Phys. Rev. B **58**, 8248 (1998).
[34] D. Alfè and M. J. Gillan, Phys. Rev. Lett. **81**, 5161 (1998).
[35] D. Alfè, G. D. Price and M. J. Gillan, Phys. Earth Planet. Inter. **110**, 191 (1999).
[36] E. Wasserman, L. Stixrude and R. E. Cohen, Phys. Rev. B **53**, 8296 (1996).
[37] A. C. Holt and M. Ross, Phys. Rev. B **1**, 2700 (1970).
[38] Y. Wang and J. Perdew, Phys. Rev. B **44**, 13298 (1991).
[39] J. P. Perdew, J. A. Chevary, S. H. Vosko, K. A. Jackson, M. R. Pederson, D. J. Singh and C. Fiolhais, Phys. Rev. B **46**, 6671 (1992).
[40] P. E. Blöchl, Phys. Rev. B **50**, 17953 (1994).
[41] G. Kresse and D. Joubert, Phys. Rev. B **59**, 1758 (1999).
[42] S. Wei and H. Krakauer, Phys. Rev. Lett. **55**, 1200 (1985).
[43] D. Alfè, M. J. Gillan and G. D. Price, Nature, **401**, 462 (1999).
[44] A. Laio, S. Bernard, G. L. Chiarotti, S. Scandolo and E. Tosatti, Science **287**, 1027 (2000).
[45] D. Vanderbilt, Phys. Rev. B **41**, 7892 (1990).
[46] N. D. Mermin, Phys. Rev. **137**, A1441 (1965).
[47] M. J. Gillan, J. Phys. Condens. Matter **1**, 689 (1989).
[48] R. M. Wentzcovitch, J. L. Martins and P. B. Allen, Phys. Rev. B **45**, 11372 (1992).
[49] G. Kresse and J. Furthmüller, Phys. Rev. B **54**, 11169 (1996).
[50] G. Kresse and J. Furthmüller, Comput. Mater. Sci. **6**, 15 (1996).
[51] H. J. Monkhorst and J. D. Pack, Phys. Rev. B **13**, 5188 (1976).
[52] G. Kresse, J. Furthmüller and J. Hafner, Europhys. Lett. **32**, 729 (1995).
[53] D. Frenkel and B. Smit, *Understanding Molecular Simulation*, Academic Press, San Diego (1996).
[54] H. C. Andersen, J. Chem. Phys. **72**, 2384 (1980).
[55] D. A. Boness and J. M. Brown, J. Geophys. Res. **95**, 21721 (1990).
[56] N. W. Ashcroft and N. D. Mermin, *Solid State Physics*, ch. 2, Holt, Rinehart and Winston, New York (1976).
[57] It is often assumed that the thermodynamic Grüneisen parameter γ is independent of temperature and depends on volume as $(V/V_0)^q$, where V_0 is a reference volume and q is a positive exponent roughly equal to unity; see e.g. O. L. Anderson, *Equations of State of Solids for Geophysics and Ceramic Science*, Oxford Monographs on Geology and Geophysics No. 31, Oxford University Press (1995).
[58] S. H. Vosko, L. Wilk and M. Nusair, Can. J. Phys. **58**, 1200 (1980).
[59] See e.g. ch. 4 of Ref. 5.
[60] We obtain the C_v values from Refs. [8,36] by using the formula given in Eqn. (10) of Ref. [8] for the electronic contribution and the Dulong-Petit value $3k_{\rm B}$/atom for the lattice contribution. The C_v values of Refs. [8,36] refer to the f.c.c. phase of Fe.
[61] T. S. Duffy and T. J. Ahrens, Geophys. Res. Lett. **20**, 1103 (1993).
[62] In contrast to Yoo *et al.* (Ref. 22), Brown and McQueen did not measure temperature in their shock experiments, but estimated it using an empirical thermodynamic relation.
[63] F. Stacey, Phys. Earth Planet. Inter. **89**, 219 (1995).

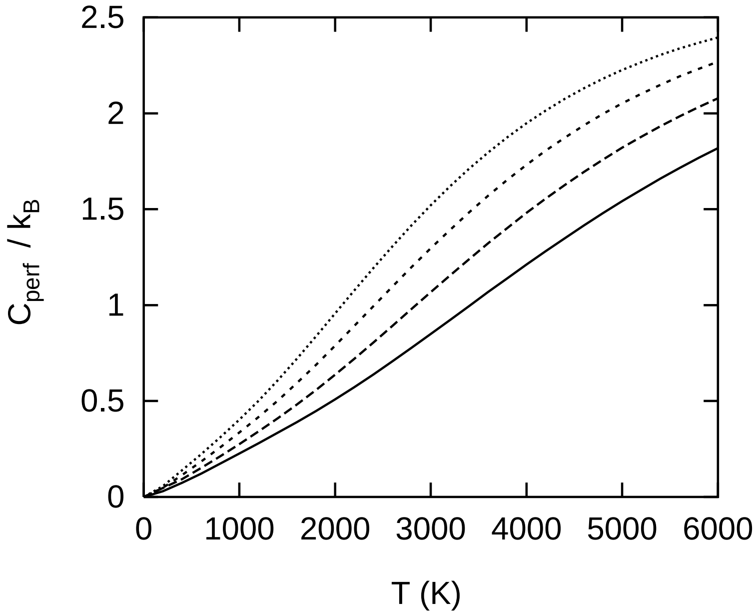

FIG. 1. Electronic specific heat per atom $C_{\rm perf}$ of the rigid perfect lattice of h.c.p. Fe (units of Boltzmann's constant $k_{\rm B}$) as a function of temperature for atomic volumes: 7.0 Å^3 (——), 8.0 Å^3 (− − −), 9.0 Å^3 (- - -) and 10.0 Å^3 (· · ·).

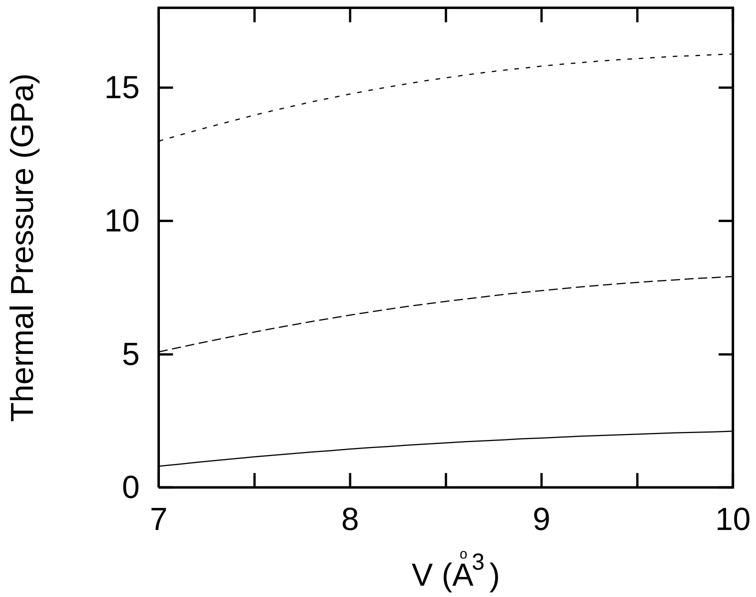

FIG. 2. Electronic thermal pressure $\Delta p_{\rm perf}$ of the rigid perfect lattice of h.c.p. Fe as a function of atomic volume V for $T = 2000$ (——), 4000 (− − −) and 6000 K (- - -).

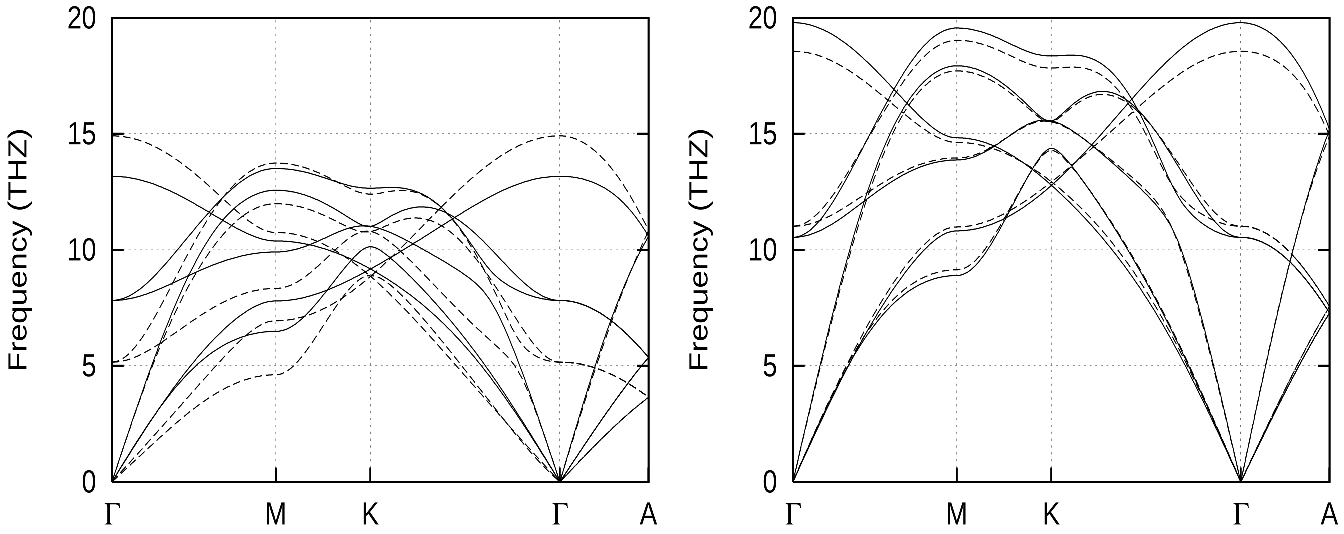

FIG. 3. Phonon dispersion relations of h.c.p. Fe calculated at atomic volumes $V = 8.67$ (left panel) and 6.97 Å^3 (right panel). Frequencies calculated directly from DFT at the two volumes are shown as solid curves. In left panel, dashed curves give frequencies from empirical inverse-power model (see text). In right panel, dashed curves show DFT frequencies for $V = 8.67$ Å^3 graphed in left panel but scaled by the factor 1.409.

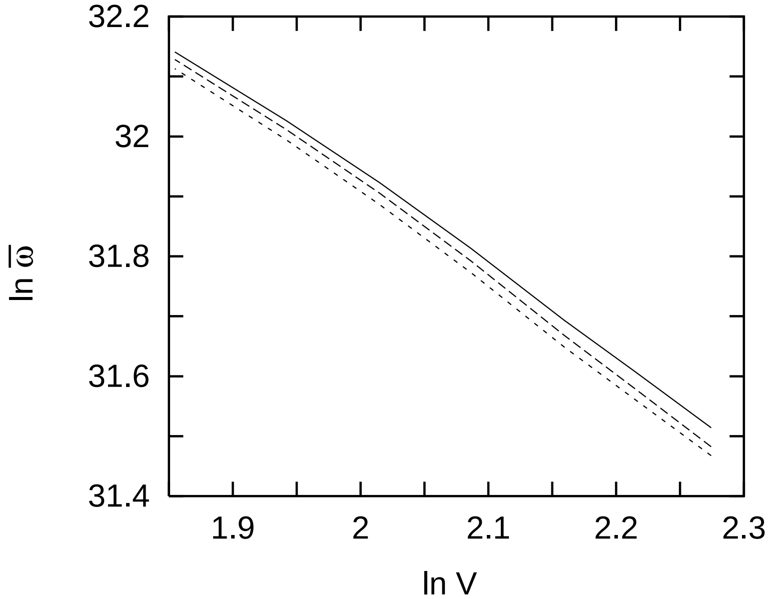

FIG. 4. Geometric-mean phonon frequency $\bar{\omega}$ of h.c.p. Fe as a function of atomic volume V for $T = 2000$ (——), 4000 (– – –) and 6000 K (- - -). The natural logarithm of the two quantities is plotted, with $\bar{\omega}$ in units of rad s^{-1} and V in units of Å^3.

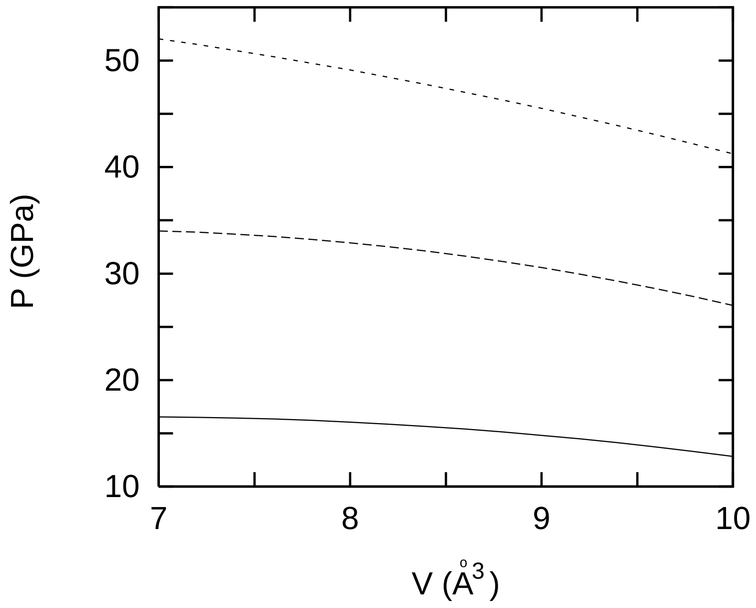

FIG. 5. The harmonic thermal pressure $p_{\rm harm}$ as a function of atomic volume V for $T = 2000$ (——), 4000 (– – –) and 6000 K (- - -).

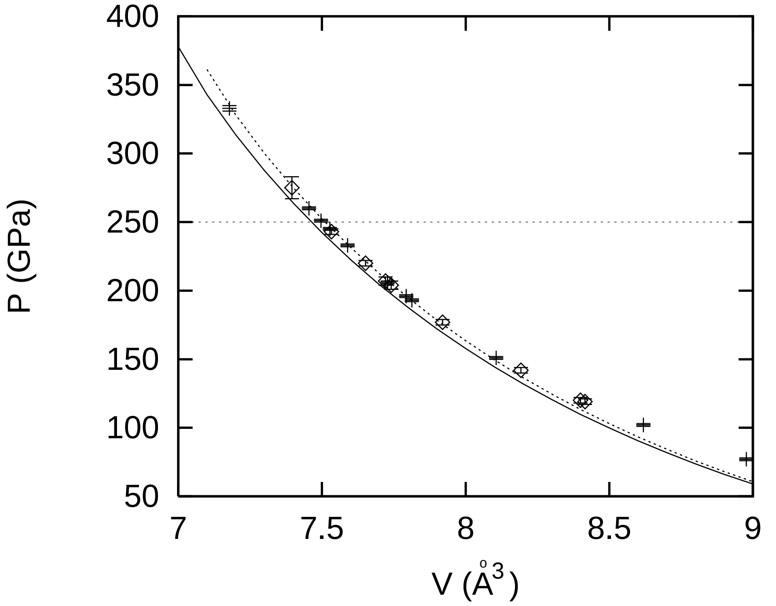

FIG. 6. Experimental and *ab initio* Hugoniot pressure p as a function of atomic volume V. Symbols show the measurements of Brown and McQueen [21]. Solid curve is *ab initio* pressure obtained when calculated equilibrium volume of b.c.c. Fe is used in the Hugoniot-Rankine equation; dotted curve is the same, but with experimental equilibrium volume of b.c.c. Fe. The comparison is meaningful only up to a pressure of *ca.* 250 GPa (horizontal dotted line), at which point the experiments indicate melting.

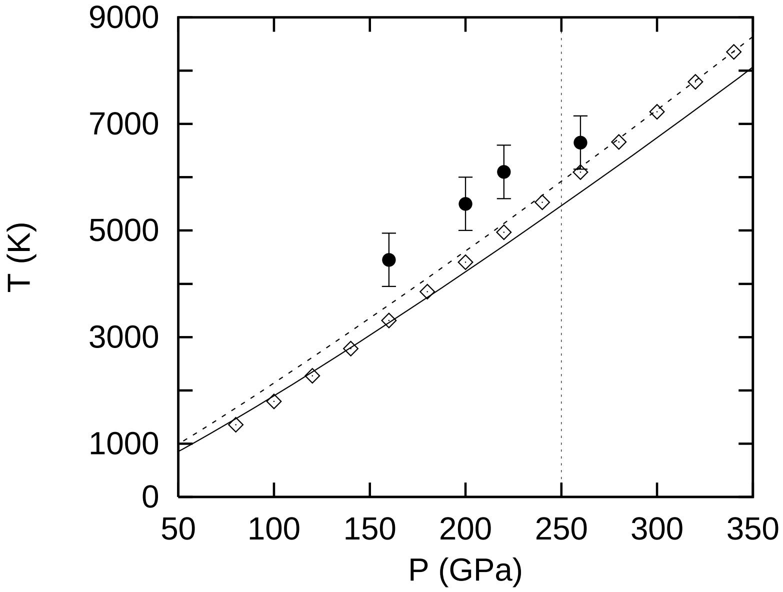

FIG. 7. Experimental and *ab initio* temperature as a function of pressure on the Hugoniot. Black circles with error bars and white diamonds are measurements due to Yoo *et al.* [22] and estimates due to Brown and McQueen [21] respectively. Solid and dashed curves are *ab initio* results obtained using theoretical and experimental b.c.c. volumes. The comparison is meaningful only up to a pressure of *ca.* 250 GPa (vertical dotted line), at which point the experiments indicate melting.

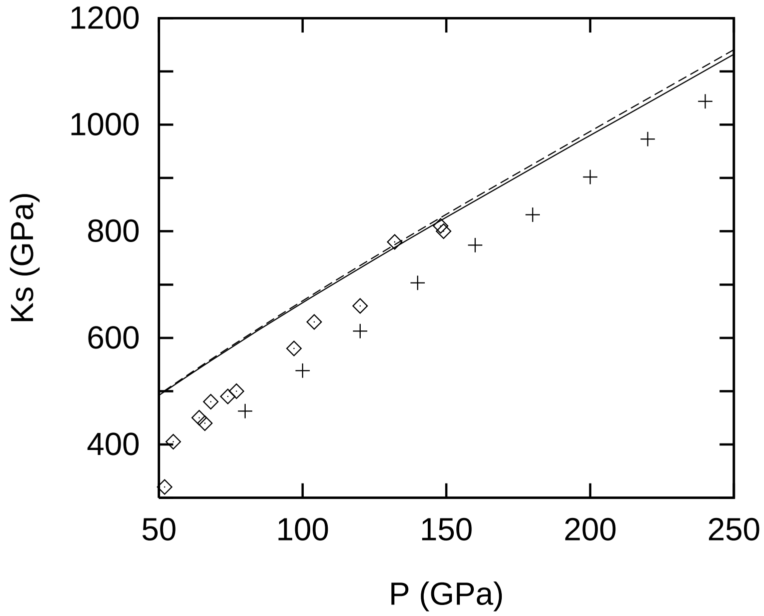

FIG. 8. Experimental and *ab initio* adiabatic bulk modulus K_S on the Hugoniot. Diamonds and pluses are measurements due to Jeanloz [20] and Brown and McQueen [21] respectively. Solid and dashed curves are *ab initio* results obtained using theoretical and experimental b.c.c. volumes.

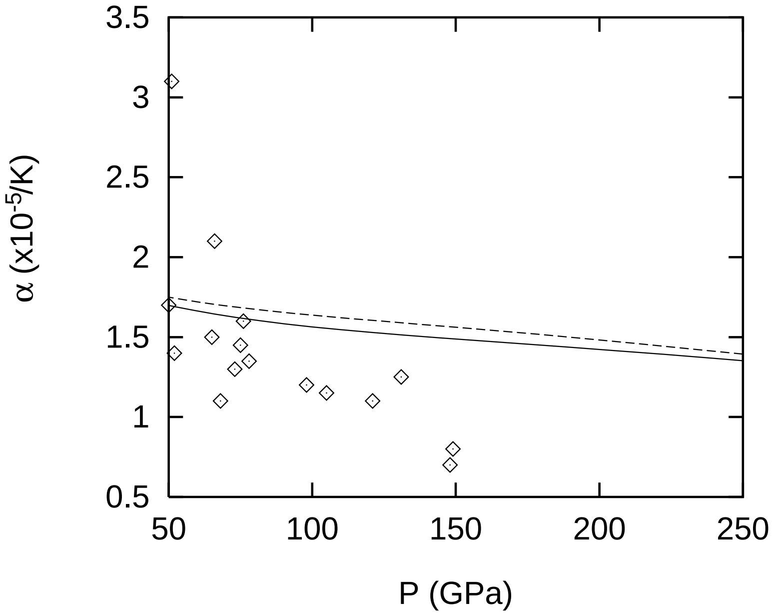

FIG. 9. Experimental and *ab initio* thermal expansivity on the Hugoniot. Diamonds are measurements due to Jeanloz [20]. Solid and dashed curves are *ab initio* results obtained using theoretical and experimental b.c.c. volumes.

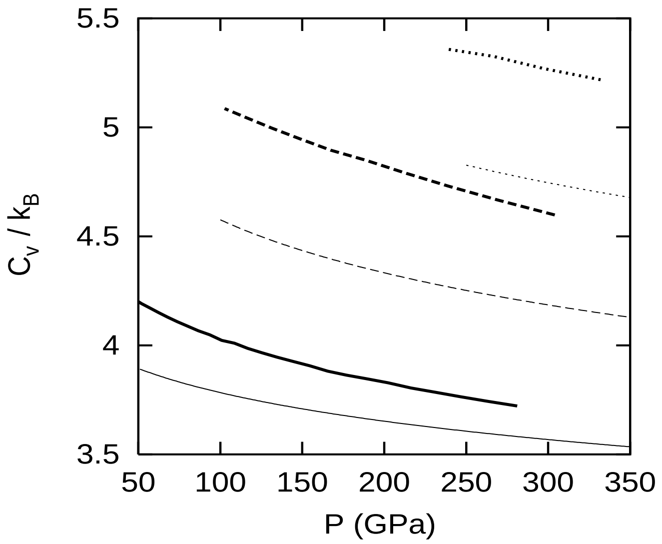

FIG. 10. Total constant-volume specific heat per atom C_v (units of $k_{\rm B}$) of h.c.p Fe as a function of pressure on isotherms T = 2000 K (continuous curves), 4000 K (dashed curves) and 6000 K (dotted curves). Heavy and light curves show present results and those of Refs. [8,36] respectively.

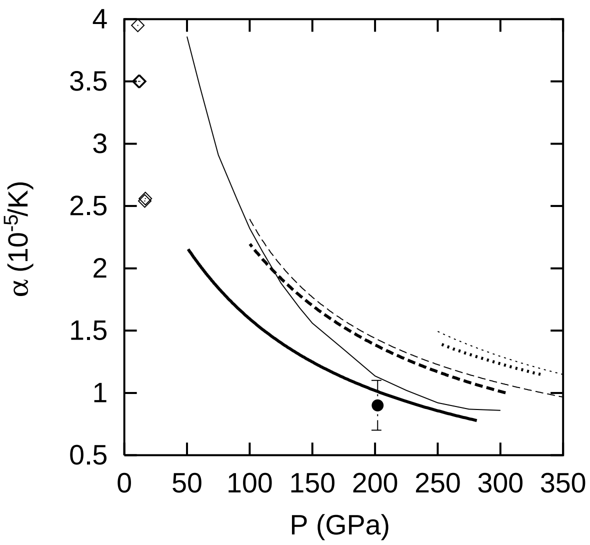

FIG. 11. Thermal expansivity α of h.c.p. Fe as a function of pressure on isotherms $T = 2000$ K (continuous curves), 4000 K (dashed curves) and 6000 K (dotted curves). Heavy and light curves show present results and those of Refs. [8,36] respectively. Black circle with error bar is experimental value of Duffy and Ahrens [61] at $T = 5200 \pm 500$ K. Diamonds are DAC values due to Boehler [10] for temperatures between 1500 and 2000 K.

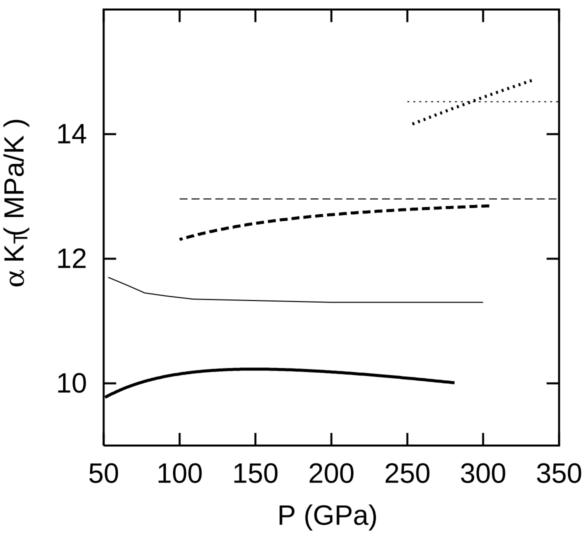

FIG. 12. Product of expansion coefficient α and isothermal bulk modulus K_T as a function of pressure on isotherms $T = 2000$ K (continuous curves), 4000 K (dashed curves) and 6000 K (dotted curves). Heavy and light curves show present results and those of Refs. [8,36] respectively.

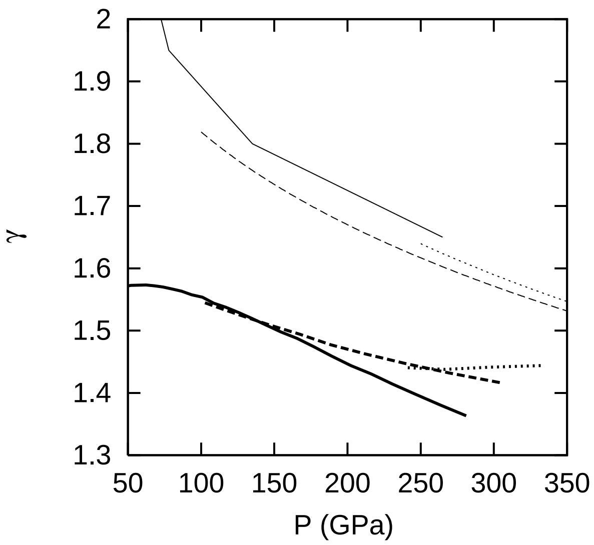

FIG. 13. Grüneisen parameter γ as a function of pressure on isotherms at $T = 2000$ K (continuous curves), 4000 K (dashed curves) and 6000 K (dotted curves). Solid and light curves show present results and those of Refs. [8,36] respectively.